Journal of Green Energy Research and Innovation

A Multi-Objective Framework for Smart Energy Hubs: Leveraging Compressed Air Storage and Demand Response

Pouria Hajiamoosha, Abdollah Rastgou, Hadi Afshar

Highlights

- **A multi-carrier energy hub generates and delivers electricity, heating, and cooling from diverse sources.**
- **The hub participates in demand response to reduce peak demand and enhance system efficiency.**
- **We use a mixed-integer linear programming approach to minimize costs and carbon emissions.**
- **Case study results demonstrate significant cost and emission reductions while improving energy hub efficiency.**

Graphical Abstract

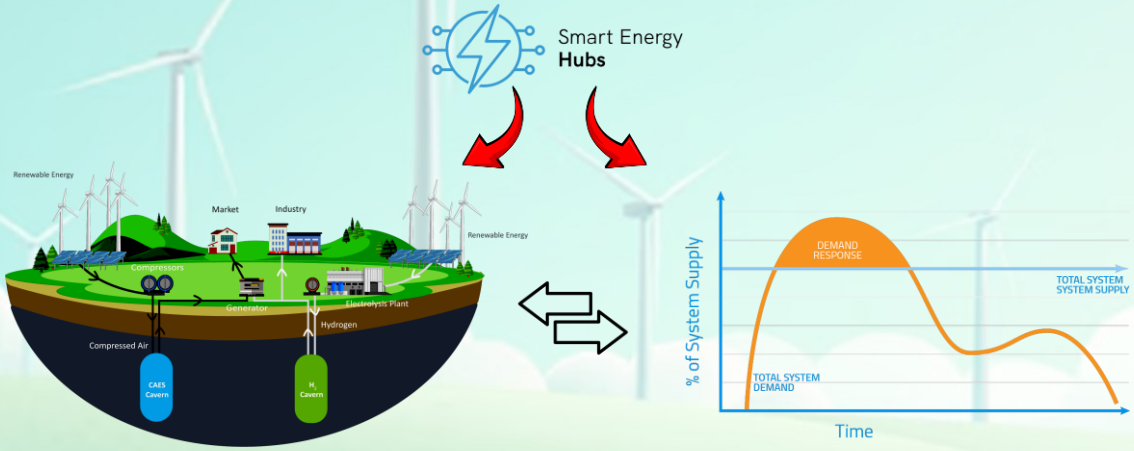

Use your device to scan and read the article online

Citation

P. Hajiamoosha, A. Rastgou, and H. Afshar," A Multi-Objective Framework for Smart Energy Hubs: Leveraging Compressed Air Storage and Demand Response," *Journal of Green Energy Research and Innovation*, vol. 2, no. 2, pp. 1-25, 2025.

https://doi.org/10.61186/jgeri.2.2.1

JGERI Journal of Green Energy Research and Innovation

Journal of Green Energy Research and Innovation 2.2 (2025) 1-25

Online ISSN: 3041-9018

Journal of Green Energy Research and Innovation

Journal Homepage: www.jgeri.araku.ac.ir

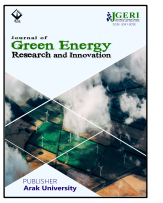

A Multi-Objective Framework for Smart Energy Hubs: Leveraging Compressed Air Storage and Demand Response

Pouria Hajiamoosha [1], Abdollah Rastgou [1,*], Hadi Afshar [2]

[1] *Department of Electrical Engineering, Kermanshah Branch, Islamic Azad University, Kermanshah, Iran.*

[2] *Electrical and Computer Engineering Faculty, Semnan University, Semnan, Iran.*

A R T I C L E I N F O

Keywords:
Energy hub,
Multi-objective programming,
Storage devices,
Optimization.

Article History:
Received: 05 March 2025;
Revised: 11 March 2025;
Accepted: 15 March 2025.

Article type:
Research Article

* ***Corresponding author***
E-mail address
abdollah.rastgou@iau.ac.ir (A. Rastgou)

A B S T R A C T

In this paper, a multi-carrier energy hub that can generate and deliver electricity, heating, and cooling energy from different sources, such as wind, solar, fuel cells, batteries, and compressed air is proposed. The intelligent energy hub can also participate in electrical and thermal demand response, which aims to reduce peak demand and enhance overall system efficiency. The scheduling problem is a mixed-integer linear programming problem that seeks to minimize the system cost and carbon dioxide emissions. To obtain optimal solutions that strike a balance between cost, emissions, and decision maker's preferences, an augmented epsilon-constraint min-max fuzzy method is employed. The proposed strategy's advantages are demonstrated through a case study, where it is compared with other methods. The results show that the proposed approach effectively reduces the cost and emissions of the smart energy hub while improving the load shape and energy hub efficiency. Moreover, the results showed that the integration of compressed air systems and demand response programs enhances the performance of the smart energy hub, making it more flexible and reliable. The GAMS software is employed for the modeling and resolution of the scheduling issue.

1. Introduction

The increasing concerns over environmental sustainability and the need for efficient utilization of energy resources have driven the development of innovative energy systems [1-3]. In recent years, numerous research studies have concentrated on the integration of various renewable energy sources, such as fuel cells, photovoltaic (PV) systems, and energy storage systems, to create hybrid energy systems [4]. These hybrid systems offer the potential for improved reliability, reduced environmental impact, and enhanced energy efficiency [5]. Nevertheless, the effective implementation and management of hybrid energy systems in practical environments present multifaceted challenges [6]. One significant challenge is the presence of demand response programs, which aim to optimize energy consumption by adjusting demand based on supply conditions. These programs introduce variability in the energy demand, thus influencing the performance and cost-effectiveness of the hybrid energy systems [7,8]. The energy hub (EH) represents a novel approach to energy systems, serving as a crucial link between diverse energy sources [9]. By enabling the smooth convergence of diverse energy systems, such as electrical grids and natural gas infrastructures, EHs foster a synchronized and effective functioning. [10]. Reference [11], proposed a microgrid that incorporates a combined heating, cooling, and power (CCHP) system, utilizing electricity and gas as energy carriers. This EH system aims to optimize the utilization of energy resources. The integration of renewable energies into the CCHP system enhances the economic and environmental aspects, which have been thoroughly investigated as delineated in [12]. In [13], the CCHP systems are studied, which employ a variety of energy suppliers, including gas turbines (GTs), gas boilers (GBs), and electric and absorption chillers, to meet the demands for heat, cooling, and power. In reference [14], a proposed EH system introduces the concept of a versatile infrastructure capable of storing and converting multiple energy carriers. In an EH framework, the requisites for cooling, power, and heating are addressed through the strategic utilization of electricity and gas, which constitute the primary energy vectors commonly in use [15]. In [16], the focus is on examining the optimization of multi-energy carriers within an EH system through the utilization of a non-linear programming model. Reference [17], presents a thorough examination of EHs in the role of decision-makers and proposes a multi-period, multi-energy operational framework designed to enhance coordination across various energy networks.

A proposed analysis of energy consumption in smart multi-energy carriers, functioning as an EH system, is presented in [18] for residential applications. In [19] Optimization of EH systems for residential loads while considering customer preferences and comfortability is solved in real time. A novel approach is presented in Reference [20] for managing the charging process of plug-in hybrid electric vehicles (PHEVs) within the structure of EHs, which utilizes a multi-objective optimization framework to determine the optimal charging patterns for PHEVs, taking into account both the perspectives of vehicle owners and system operators. Reference [10] has developed a residential EH model that demonstrates the operation of multiple energy carriers in a home. They propose an integrated infrastructure and an optimization problem to enhance the performance of a smart home.

Demand response (DR) programs are becoming increasingly prevalent in the context of microgrids. These programs allow for the efficient management and utilization of energy resources by adjusting consumer demand to match the available supply. By engaging participants to temporarily reduce or shift their energy consumption during peak periods, DR programs optimize the overall operation of the EH. Through intelligent communication and control systems, these programs enable the seamless integration of distributed energy resources, such as solar panels and battery storage, into the grid, providing a reliable and sustainable solution for the ever-increasing energy demand. Reference [21] and [22] have studied DR programs in multi-energy systems. In [23], the DR program and energy generation for various customer types in a microgrid are modeled using a two-stage stochastic function. A stochastic energy procurement model that considers the effects of DR is proposed in reference[24]. This model is designed for large electricity consumers and demonstrates operational cost reductions by shifting the load from peak to off-peak periods. Reference [25] presents a concept of electricity shifting potential to determine the maximum reduction of electricity from the grid to the distributed multi-generation system, based on a profitability map of DR incentives. The optimal solutions and scheduling in DR in multi-energy carriers have been investigated in fewer studies compared with studies that investigate the potential and modeling analysis of DR in multi-energy carriers. In [26], the economic performance of the gas-fired CCHP system is thoroughly examined, taking into account various factors that influence its overall efficiency. A sensitivity analysis is also conducted to assess the system's robustness under different scenarios.

The motivation of this paper is to develop a model of a smart grid in the EH concept in which different forms of energy such as power, heat, and cold, are integrated into it, and different energy carriers such as gas and electricity support the EH with the different multi-generation unit are in the model. This paper proposes a scheduling strategy for a smart multi-carrier EH (SMEH) that can provide electricity, heating, and cooling from various sources. The SMEH includes a wind turbine (WT), a solar panel, a micro-turbine, a fuel cell, a boiler, an absorption chiller, a battery, and a compressed air energy storage (CAES) system. The SMEH can also join electrical and thermal DR programs to lower the peak demand and improve the system's efficiency. We model the scheduling problem as a mixed-integer linear programming (MILP) problem that aims to minimize the system cost, carbon dioxide emissions, and risk. We solve the problem using an augmented epsilon-constraint min-max fuzzy method that can produce optimal solutions that balance the different objectives and the decision maker's preferences. We present three case studies to show the benefits of the proposed strategy and to compare it with other methods. We also discuss using GAMS software to model and solve the scheduling problem. Two objective functions are addressed for this multi-objective optimization problem, first operation cost and second carbon emission reduction. The argument epsilon constraint method is implemented to solve multi-objective problems and obtain the optimal Pareto solutions. The epsilon constraint method offers significant advantages over other methods, such as the weighted sum method. The epsilon constraint method provides a more comprehensive explanation of the solutions on the Pareto front. Different methods are employed to select an optimal solution from the Pareto front, ensuring a balanced tradeoff between objectives. The max-min fuzzy technique is particularly effective for this purpose. Additionally, two distinct DR programs, real-time pricing (RTP) and Time-of-Use (TOU), are implemented to optimize operational costs and reduce carbon emissions [27].

The paper's contributions are succinctly summarized as follows:

- Establishment of a Comprehensive Framework: Integration of WT, PV, and CCHP systems, alongside electric heat pumps (EHP) and CAES units within an EH system.
- Optimal multi-objective model: development of a model addressing both economic and environmental challenges.
- Epsilon constraint method: the application of the epsilon constraint method addresses the multi-objective optimization problem effectively.
- Max-min fuzzy technique: the max-min fuzzy technique is utilized to derive a compromise solution.
- Reduction of operation costs and carbon emissions: implementing RTP and TOU-DR programs leads to the reduction of operational costs and carbon emissions, achieving simultaneous cost savings and environmental benefits.
- Mixed-integer linear programming: The application of mixed-integer linear programming techniques guarantees the derivation of the most efficient solution for the specified problem.

2. Problem formulation

2.1. Mathematical formulation for an energy hub system

Operation cost minimization is considered the first objective of the model as shown in Equation (1):

$$F(\mathrm{Cos}t) = \sum_{t=1}^{T} (C_{pg}(t) + C_{pe}(t) + SUC_{CHP}(t) + SDC_{CHP}(t)) \quad (1)$$

The second objective function is minimizing carbon emissions as shown in Equation (2).

$$F(Emission)=\sum_{t=1}^{T}(E_{pg}(t)+E_{pe}(t)) \tag{2}$$

where:

$$C_{pg}^{t}=P_{g}\times(P_{ge}^{t}+P_{gh}^{t}+P_{gchp}^{t}+P_{gcaes}^{t}) \tag{3}$$

$$C_{pe}^{t}=P_{e}^{t}\times(P_{buy}^{t}-P_{sell}^{t}) \tag{4}$$

$$E_{pg}^{t}=P_{g}\times\beta_{g}\times(P_{ge}^{t}+P_{gh}^{t}+P_{gchp}^{t}+P_{gcaes}^{t}) \tag{5}$$

$$E_{pe}^{t}=\eta_{t}\times P_{buy}^{t} \tag{6}$$

The power hub is capable of bi-directional energy transfer with the electrical grid, allowing for both the absorption and distribution of power. Exchanging power between the grid and EH is modeled as Equation (7):

$$P_{grid}^{t}\eta_{t}=P_{sell}^{t}+P_{buy}^{t} \tag{7}$$

The gas turbine model indicates that it comprises the GT power supply heat exchanger and the power hub. The representation of the GT model is as Equation (8):

$$P_{ge}^{t}\eta_{ge}=P_{gt}^{t} \tag{8}$$

The capacity limitations of different devices are presented in Equation (9)-(16).

$$0\le P_{pv}^{t}\le P_{pv}^{\max} \tag{9}$$

$$0\le P_{wt}^{t}\le P_{wt}^{\max} \tag{10}$$

$$0\le P_{gas}^{t}\le P_{gas}^{\max} \tag{11}$$

$$0\le P_{gt}^{t}\le P_{gt}^{\max} \tag{12}$$

$$P_{chp}^{\min}\le P_{chp}^{t}\le P_{chp}^{\max} \tag{13}$$

$$-P_{grid}^{\max}\le P_{grid}^{t}\le P_{pv}^{\max} \tag{14}$$

$$T_{EHP}^{\min}\le T_{EHP}^{t}\le T_{EHP}^{nax} \tag{15}$$

$$PS^{\min}\le PS^{t}\le PS^{\max} \tag{16}$$

The cooling section's energy conversion model outlines technical constraints, including the unidirectional reception of cooling energy from both electric and absorption chillers. The absorption chiller utilizes heat, while the electric chiller uses electricity to produce cooling.

The mathematical models for the electric and absorption chillers are outlined in Equation (17) and (18), respectively [27].

$$P_{ec}^{t}COP_{ec}=C_{ec}^{t} \tag{17}$$

$$H_{ac}^{t}COP_{ac}=H_{ac}^{t} \tag{18}$$

The ice storage air conditioning system, a critical element of the cooling infrastructure, is composed of a chiller unit and an ice storage tank. The chiller's role is to produce ice, while the tank is responsible for its storage and subsequent melting during peak demand periods. The implementation of intelligent storage co1000ntrol enables the efficient redistribution of electrical loads, shifting them from peak to off-peak periods, as documented in [28]. This shift in consumption patterns leads to a reduction in load variations, ensuring a more stable and balanced energy demand. Additionally, Reference [29] explores the optimization of ice storage tank efficiency and life cycle costs, providing valuable insights that enhance the system's overall effectiveness and economic viability.

The balance of cooling energy produced is detailed in Equation (19). The inequalities presented in Equation (20) and Equation (21) delineate the capacity limitations of the ice storage air conditioner and the electrical chiller, respectively.

$$P_{ice}^{t}COP_{ice}=P_{cs,c}^{t} \tag{19}$$

$$0\le P_{ice}^{t}\le P_{ice}^{\max} \tag{20}$$

$$0\le P_{ac}^{t}\le P_{ec}^{\max} \tag{21}$$

2.2. The thermal section energy conversion model

The Equation (22) illustrates the equilibrium of gas input within the EH system.

$$P_{gas}^{t}=P_{ge}^{t}+P_{chp}^{t}+P_{gh}^{t}+P_{caes}^{t} \tag{22}$$

The energy conversion process of the GB is delineated in Equation (23), where the output heat is transferred to the heating hub.

$$\eta_{gh,gb}P_{gh}^{t}=H_{gb}^{t} \tag{23}$$

The energy conversion of the GT is detailed in Equation (24), with the resultant heat being directed to the heat exchanger.

$$\eta_{gh,gt} P_{ge}^{t} = H_{gt}^{t} \tag{24}$$

The heat exchanger's output is then utilized by the heating hub. Equation (25) outlines the operational constraints of the GB, ensuring it operates at no less than 25% of its maximum capacity throughout all time horizon periods. Additionally, Equation (26) describes the limitations of the air conditioner (AC), where a deliberately reduced AC capacity results in a correspondingly lower cooling output.

$$0.25 \times H_{gb}^{\max} \le H_{gb}^{t} \le H_{gb}^{\max} \tag{25}$$

$$0 \le H_{ac}^{t} \le H_{ac}^{\max} \tag{26}$$

Equation (27) establishes the principle of energy parity within the power hub, stipulating that the sum of energy inputs must equate to the sum of energy outputs, with the left side of the equation representing the input power and the right side detailing the output power.

$$P_{buy}^{t} + P_{pv}^{t} + P_{wt}^{t} + P_{gt}^{t} + P_{es,d}^{t} + P_{chp}^{t} + P_{gen.}^{t} = P_{ec}^{t} + P_{es,c}^{t} + P_{ice}^{t} + P_{echp}^{t} + P_{con.}^{t} + PL^{t} \tag{27}$$

For the cooling hub, Equation (28) articulates the interplay between the absorption chiller, electric chiller, and the cold energy discharge from the intelligent storage control, which collectively meets the cooling demand detailed on the right side of the equation.

$$C_{ac}^{t} + C_{ec}^{t} + P_{cs,d}^{t} = CL^{t} \tag{28}$$

Additionally, Equation (29) defines the balance of heat exchange within the heating hub.

$$\eta_{he} H_{gt}^{t} + H_{gb}^{t} + P_{hs,d}^{t} + T_{chp}^{t} + T_{ehp}^{t} + T_{tr}^{t} = H_{ac}^{t} + P_{hs,c}^{t} + HL^{t} \tag{29}$$

2.3. Energy storage model

System inefficiencies often stem from elevated energy prices during peak load times. Integrating storage devices into the EH system can mitigate this issue by leveraging off-peak charging and peak-hour discharging to lower operational costs and CO_2 emissions. The utility of electric vehicles as energy storage solutions is examined in [30]. Reference [31] proposes a comprehensive model encompassing electricity, heating, and cooling energy storage systems. The operational parameters for electrical storage devices are formulated in Equation (30)-(34) [27].

$$E_{es}^{t+1} = E_{es}^{t}(1-\delta_{es}) + \left(P_{es,c}^{t}\eta_{es,c} - \frac{P_{es,d}^{t}}{\eta_{es,d}} \right) \tag{30}$$

$$0 \le P_{es,c}^{t} \le u_{es}.P_{es,c}^{\max} \tag{31}$$

$$0 \le P_{es,d}^{t} \le (1-u_{es}).P_{es,d}^{\max} \tag{32}$$

$$E_{es}^{\min} \le E_{es}^{t} \le E_{es}^{\max} \tag{33}$$

$$E_{es}^{24} = E_{es}^{0} \tag{34}$$

Equation (30) represents the stored energy in the electrical storage (ES) system based on its charging and discharging modes. The charging and discharging modes of electrical storage, along with their limitations, are expressed in Equation (31) and (32), respectively. A binary variable is introduced to prevent simultaneous charging and discharging. Equation (33) defines the limitation of stored energy. Additionally, Equation (34) ensures that the energy amounts in the first and last hours of the time horizon are equal [27]. For cooling storage devices, the equations are expressed in Equation (35)-(39).

$$E_{cs}^{t+1} = E_{cs}^{t}(1-\delta_{cs}) + \left(P_{cs,c}^{t}\eta_{cs,c} - \frac{P_{cs,d}^{t}}{\eta_{cs,d}} \right) \tag{35}$$

$$0 \le P_{cs,c}^{t} \le u_{cs}.P_{cs,c}^{\max} \tag{36}$$

$$0 \le P_{cs,d}^{t} \le (1-u_{cs}).P_{cs,d}^{\max} \tag{37}$$

$$E_{cs}^{\min} \le E_{cs}^{t} \le E_{cs}^{\max} \tag{38}$$

$$E_{cs}^{24} = E_{cs}^{0} \tag{39}$$

Equation (35) represents the stored energy in CS based on its charging and discharging mode. Charging and discharging modes of electrical storage and their limitations are expressed in Equation (36) and (37) respectively. Incorporating the binary variable can ensure that the processes of charging and discharging are mutually exclusive. Equation (38) defines the constraints on the amount of energy that can be stored. To balance the energy levels at the beginning and end of the planning horizon, Equation (39) is introduced. For electrical storage devices, the equations are expressed in Equation (40)-(44).

$$E_{hs}^{t+1} = E_{hs}^{t}(1-\delta_{hs}) + \left(P_{hs,c}^{t}\eta_{hs,c} - \frac{P_{hs,d}^{t}}{\eta_{hs,d}} \right) \tag{40}$$

$$0 \le P_{hs,c}^{t} \le u_{hs}.P_{hs,c}^{\max} \tag{41}$$

$$0 \le P_{hs,d}^{t} \le (1-u_{hs}).P_{hs,d}^{\max} \tag{42}$$

$$E_{hs}^{\min} \le E_{hs}^{t} \le E_{hs}^{\max} \tag{43}$$

$$E_{hs}^{24} = E_{hs}^{0} \tag{44}$$

Equation (40) represents the stored energy in the heat storage (HS) system based on its charging and discharging modes. The charging and discharging modes of electrical storage, along with their limitations, are expressed in Equation (41) and (42), respectively. A binary variable is introduced to prevent simultaneous charging and discharging. Equation (43) defines the limitation of stored energy. Additionally, Equation (44) ensures that the energy amounts in the first and last hours of the time horizon are equal.

2.4. Operation cost and constraints for CHP unit

CHP technologies are one of the most used units in smart and multi-carrier systems [9]. CHP units are recovering thermal to gain more performance and use wasted thermal energy for local heating. Power and thermal outputs in CHPs depend on each other and cannot change separately. CHP energy conversion is shown in Equation (45) and Equation (46).

$$\eta_{chp} \times P_{gchp}^{t}(t) = P_{chp}(t) \tag{45}$$

$$T_{chp}(t) = P_{chp}(t) \times HPR \times \eta_{He} \tag{46}$$

Equation (47) and (48) represent CHP power and thermal ramp-up and ramp-down constraints, respectively.

$$P_{chp}(t) - P_{chp}(t-1) \le P^{Ramp-up} \times \gamma_{t-1} \times i_t \times P_{chp}^{\min} \tag{47}$$

$$P_{chp}(t) - P_{chp}(t-1) \le P^{Ramp-up} \times \gamma_{t-1} \times i_t \times P_{chp}^{\min} \tag{48}$$

The CHP start-up and shut-down costs are shown in Equations (49) and (50), respectively. Equation (51)-(55) are employed to model CHP on and off mode [9].

$$SUC(t) = SU \times i(t) \tag{49}$$

$$SDC(t) = SD \times j(t) \tag{50}$$

$$0 \le i(t) \le \gamma(t) \tag{51}$$

$$\gamma(t) - \gamma(t-1) \le i(t) \le 1 - \gamma(t-1) \tag{52}$$

$$0 \le j(t) \le \gamma(t-1) \tag{53}$$

$$\gamma(t-1) - \gamma(t) \le j(t) \le 1 - \gamma(t) \tag{54}$$

$$\gamma(t-1) - \gamma(t) + i(t) - j(t) = 0 \tag{55}$$

2.5. Electrical heat pump constraints

Equation (56) represents the EHP system constrains.

$$T_{EHP}^{t} = P_{EHP}^{t} \times COP_{EHP} \tag{56}$$

2.6. CAES system constraints

Conventional natural GT generators serve as the foundation of the CAES technology. Within the CAES system, high-pressure compressed air is utilized as a form of stored energy, which can be converted into various types of energy. During off-peak periods, compressors in the CAES system compress air to high-pressure levels, which is then used during peak periods to drive an expander for electricity generation to meet high electrical demands. The injection of air into the CAES system is proposed in Equation (57) in [27]. Equation (57) and Equation (59) demonstrate the power produced by the CAES system based on the pumping of air and gas consumption, respectively. The constraints on pumping air into a chamber and injecting air into storage are formulated in Equation (60) and Equation (61), respectively. To prevent simultaneous injection and pumping in the CAES system, binary variables are introduced in Equation (62). It represents the thermal recovery of the CAES unit.

$$V_{injected}^{t} = e^{i} \times P_{cons.}^{t} \tag{57}$$

$$P_{gen.}^{t} = e^{p} \times V_{pumped}^{t} \tag{58}$$

$$P_{gen}^{t} = P_{caes}^{t} / \eta_{pcaes} \tag{59}$$

$$V_{pumped}^{\min} \times h^{t} \le V_{pumped}^{t} \le V_{pumped}^{\max} \times h^{t} \tag{60}$$

$$V_{ingected}^{\min} \times f^t \le V_{ingected}^t \le V_{ingected}^{\max} \times f^t \quad (61)$$

$$f^t + h^t \le 1 \quad (62)$$

$$P_{gen.}^t \times \eta_{tr} = T_{tr}^t \quad (63)$$

The distribution of air stored within specific time intervals is influenced by the inflow and outflow of air, a relationship which can be mathematically represented as Equation (64).

$$PS^{t+1} = PS^t + V_{injected}^t - V_{pumped}^t \quad (64)$$

The heat rate is a measure of the quantity of natural gas utilized for each unit of peak electrical energy produced by the expander [32].

2.7. Electric load with demand response

DR methods are used to prevent unnecessary capacity investment by shifting loads from peak and expensive periods to off-peak and inexpensive periods [30]. In this article, TOU and RTP methods are used to implement DR programs as follows:

2.8. TOU-DR formulation

The TOU demand response (TOU-DR) and the respective models are expressed by Equation (65) and Equation (66).

$$Pl_{DR}^t = Pl_D^t + ldr^t \quad (65)$$

$$ldr_t = DR_t \times Pl_t^d \quad (66)$$

Where Pl_t^{DR} is representing new power demand of hour t by applying TOU-DR and ldr_t is the amount of shifted load in hour t and the total amount of shifted load over a daily period should be equal to zero. This is expressed in Equation (67) and at each time period shifted load is limited by Equation (68).

$$\sum_{t=1}^{24} ldr_t = 0 \quad (67)$$

$$DR_t^{\min} \le DR_t \le DR_t^{\max} \quad (68)$$

2.9. RTP-DR programming

An RTP model, constructed from electricity load demand data, facilitates the implementation of the DR program in this sector. The application of RTP-based DR encourages the shifting of loads from peak to off-peak periods, resulting in a more uniform load demand curve.

Equation (69) represents the total electrical load demand of the EH and in Equation (70), P_{av}, is the average electricity demand.

$$W_d = \sum_{t=1}^{24} PL_t \quad (69)$$

$$P_{av} = \frac{W_d}{24} \quad (70)$$

The RTP float factor is considered as Equation (71).

$$\gamma_t = \frac{Pl_t}{Pl_{av}} \quad (71)$$

The RTP model is expressed in Equation (72) and Equation (73) as follows:

$$\lambda_{RTP}^t = \gamma_t \times \lambda_{TOU}^t \quad (72)$$

$$\lambda_{RTP}^{\min} \le \lambda_{RTP}^t \le \lambda_{RTP}^{\max} \quad (73)$$

In Reference [33], the effects of employing various DR methods based on price and incentive are investigated within the EH system. References [34,35] propose a mathematical formulation for demand response, which is encapsulated in Equation (74).

$$Pl_{RTP}^t = Pl^t + E \times Pl^t \left(\frac{\lambda_{RTP}^t - \lambda_{TOU}^t}{\lambda_{TOU}^t} \right) \quad (74)$$

3. Methodology

3.1. Augmented Epsilon-constraint method

The Augmented Epsilon-constraint method has been employed to achieve more precise results in the energy management problem. The advantages of this method can be summarized as follows:

1. The original feasible region will not be altering
2. non-inferior solutions are produced, and solutions will be independent of the scaling of the objective functions.

To implement the Epsilon method, the objective function is defined as Equation (75):

$$\begin{aligned} &\max\left(f_1(x)+\delta\left(s_1+\ldots+s_p\right)\right)\\ &subject\ to\\ &f_2(x)-s_2=e_2\\ &f_3(x)-s_3=e_3\\ &\ldots\\ &f_p(x)-s_p=e_p\\ &x\in s\ \ and\ \ s_i\in R^+ \end{aligned} \tag{75}$$

Equation (75) provides efficient solutions, while the proposed method has other alternative solutions. On the other hand, there is an answer like x, that dominates other answers. As a result, this issue is defined as Equation (76):

$$\begin{cases} e_2+s_2\le e_2+s_2'\\ e_3+s_3\le e_3+s_3'\\ \ldots\\ e_p+s_p\le e_p+s_p' \end{cases} \tag{76}$$

Equation (76) can be achieved considering at least one strict inequality regarding Equation (77).

$$\sum_{i=2}^{p} S_i \le \sum_{i=2}^{p} S_i' \tag{77}$$

In order to circumvent potential scaling complications, it is better to replace s_i with s_i/r_i. As a result, the objective function converts to Equation (78).

$$\max\left(f_1(x)+eps\times(s_2/r_2+\ldots+s_p/r_p)\right) \tag{78}$$

Equation (78) is the final equation used to solve a multi-objective problem. X, $f_p(x)$, s, r_i, and are a vector of decision variables, p objective functions, feasible region, and range of its objective function, respectively.

3.2. Decision-making

Reference [27], examines various methodologies for resolving multi-objective models, including the epsilon constraint method, the weighted sum approach, and evolutionary algorithms. This paper employs the epsilon constraint argument to address the multi-objective model. Additionally, the max-min fuzzy satisfying technique is utilized (Equation (79)) to standardize the dimensions across all objective function values, as detailed subsequently.

$$\mu_k^n=\begin{cases} 1 & f_k^n\le f_k^{\min}\\ \dfrac{f_k^{\max}-f_k^n}{f_k^{\max}-f_k^{\min}} & f_k^{\min}\le f_k^n\le f_k^{\max}\\ 0 & f_k^n\ge f_k^{\max} \end{cases} \tag{79}$$

$$\mu^n=\min(\mu_1^n,\ldots,\mu_n^n) \tag{80}$$

$$\mu^{\max}=\max(\mu^1,\ldots,\mu^{np}) \tag{81}$$

The selection of the minimum quantities of the Pareto solution is described by Equation (80), whereas Equation (81) expresses the attainment of the maximum value among the minimum solutions, signifying the compromise solution.

4. Numerical results

In this section, the initial part presents the input data and parameters for the EH. Then, the min-max fuzzy method is employed to identify the optimal solution for each case study. This method is applied after utilizing the argument epsilon constraint method to obtain a set of potential solutions. By comparing these solutions, the most suitable one is selected as the optimal solution for each of the three case studies. The first case study does not incorporate any DR program. However, the second case study examines the impact of TOU programs. Similarly, the third case study focuses on the effects of RTP DR programs. Within this section, the input parameters for the model components and energy carriers are presented. The output power generated by the PV and WT systems over 24 hours is depicted in Figure 1. Figure 2 illustrates the power, cooling, and heating energy demand during the optimization time horizon on a typical hot day. Figure 3 represents the Power load with and without DRPs. Figure 4 represents the electricity

tariff of TOU, RTP use, and gas prices. Tables 1-3 provide an overview of the parameters of coefficients, including those for CCHP, EHP, CAES, WT, PV, and carbon emissions. Additionally, Table 4 presents parameters for cooling, heating, and power storage devices. Lastly, Table 5 outlines the DR parameters. It is worth noting that the CHP unit is initially considered off.

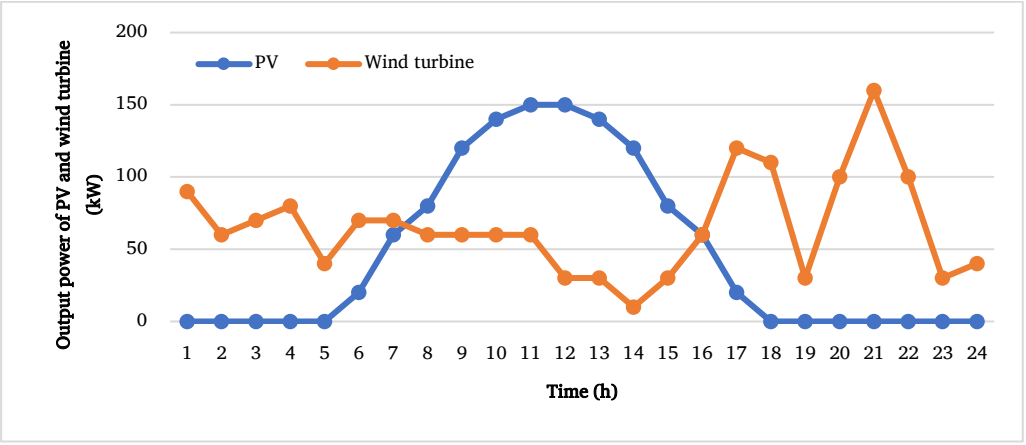

Figure 1. The output powers of WT and PV.

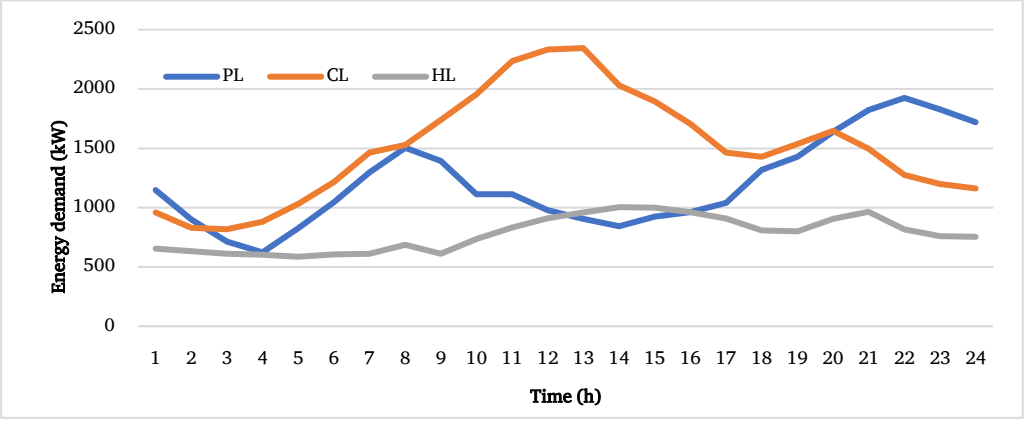

Figure 2. The power, cooling, and heating demands of the microgrid on a typical summer day.

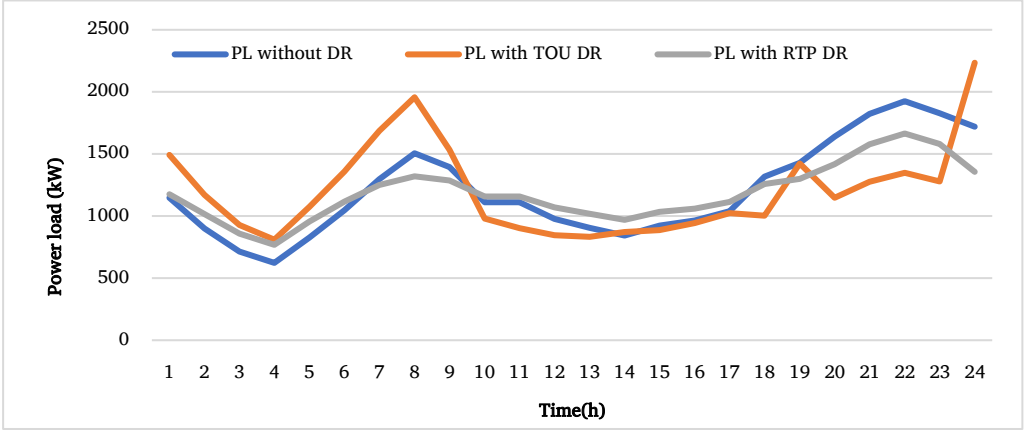

Figure 3. Power load with and without DRP.

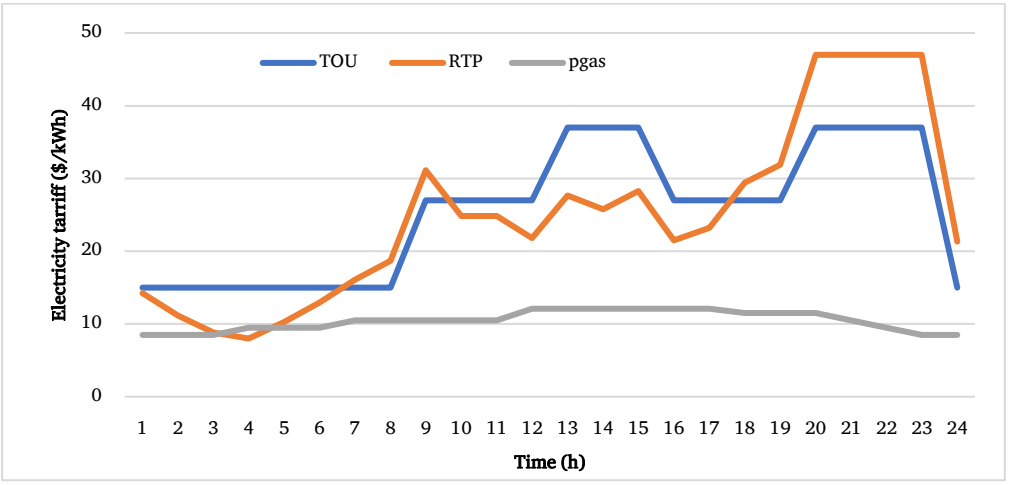

Figure 4. Electricity tariff of TOU, RTP, and gas price.

Table 1. Parameters of coefficients of CCHP, WT, PV, and Carbon emission

Parameter	Unit	Value	parameter	Unit	Value	parameter	Unit	Value
$P_{gt}^{\max}$	kW	1000	$P_{grid}^{\max}$	kW	1500	COP_{ec}	-	4
$H_{gb}^{\max}$	kW	800	$P_{gas}^{\max}$	kW	3400	COP_{ice}	-	3.5
$H_{ac}^{\max}$	kW	500	η_{ge}	-	0.3	COP_{ac}	-	1.2
$P_{ec}^{\max}$	kW	500	$\eta_{gh,gb}$	-	0.9	β_e	Kg/kWh	0.972
$P_{ice}^{\max}$	kW	100	$\eta_{gh,gt}$	-	0.4	β_g	Kg/kWh	0.23
$P_{pv}^{\max}$	kW	180	η_t	-	0.98	E	-	-0.5
$P_{wt}^{\max}$	kW	200	η_{he}	-	0.7		-	

Table 2. Parameters of CHP unit and CAES system.

CHP UNIT		CAES SYSTEM	
Capacity (kW)	1000	Maximum/ minimum level (kWh)	500/50
Electrical ramp-up/ramp-down (kW/h)	150	Maximum level of injected air (kW/h)	150
Startup/ shutdown cost ($)	65	Minimum level of injected air (kW/h)	5
Electrical/thermal conversion efficiency (%)	45/48	Maximum level of pumped air (kW/h)	150
		Minimum level of pumped air (kW/h)	5
		Efficiency of injected/produced power (%)	90/90

Table 3. Parameters of the EHP system.

Coefficient of performance	2.5
Maximum capacity (kW)	250
Minimum capacity (kW	0

Table 4. Parameters of storage devices.

Electrical storage parameters			Heat storage parameters			Cool storage parameter		
Parameter	Unit	Value	Parameter	Unit	Value	Parameter	Unit	Value
$P_{es,c}^{\max}$	kW	500	$P_{hs,c}^{\max}$	kW	800	$P_{cs,c}^{\max}$	kW	700
$P_{es,d}^{\max}$	kW	700	$P_{hs,d}^{\max}$	kW	800	$P_{cs,d}^{\max}$	kW	800
$E_{es}^{\min}$	kW	400	$E_{hs}^{\min}$	kW	400	$E_{cs}^{\min}$	kW	400
$E_{es}^{\max}$	kW	1800	$E_{hs}^{\max}$	kW	1800	$E_{cs}^{\max}$	kW	1800
$\eta_{es,c}$	-	0.96	$\eta_{hs,c}$	-	0.98	$\eta_{cs,c}$	-	0.97
$\eta_{es,d}$	-	0.96	$\eta_{hs,d}$	-	0.98	$\eta_{cs,d}$	-	0.95
δ_{es}	-	0.01	δ_{hs}	-	0.02	δ_{cs}	-	0.02

Table 5. TOU and RTP DR parameters.

$\lambda_{RTP}^{\min}$	8
$\lambda_{RTP}^{\max}$	47
E	-0.5
$DR_t^{\min}$	-30%
$DR_t^{\max}$	30%

4.1. A comparative analysis of Pareto results and the trade-off solution across three cases

In this section, an examination is conducted of the EH system model through three distinct case studies. The objective is to address the problem using the augmented epsilon constraint method, thereby showcasing the benefits and effectiveness of the proposed model as a solving technique. Figure 5 shows the Pareto solutions for scenarios with and without DRPs.

The first case study focuses on minimizing both the total cost and emissions in the EH System without any DR programs. Analyzing the system under this scenario allows for a comprehensive understanding of the baseline performance and serves as a benchmark for comparison with the subsequent cases. Moving on to the second case study, the aim remains the same to minimize the total cost and emissions in the EH system.

However, this time, the analysis considers the presence of RTP DR programs. These programs introduce a dynamic element to the system, as the pricing varies based on real-time demand. By considering this factor, the model can optimize the system's performance under these conditions. Lastly, the third case study delves into the optimization of the EH System by considering the time of use pricing DR programs. This means that the model considers the specific time periods during which the DR programs are active. By incorporating this temporal aspect, the model can further refine its optimization strategy and achieve even greater efficiency in minimizing both the total cost and emissions. Overall, these three case studies provide a comprehensive analysis of the EH system model and its solving method. Examining the system under different scenarios allows for a thorough evaluation of its advantages and efficiency in optimizing the total cost and emissions.

In case one, each component of the EH and energy carriers possesses distinct specifications in terms of cost and emissions, resulting in diverse behaviors within each Pareto front optimal solution. To derive the Pareto-optimal solutions, the epsilon constraint method is applied. Subsequently, the max-min fuzzy technique is employed to determine an optimal trade-off solution among the derived solutions. The outcomes are depicted in Figure 5. In the EH model for case study one, the operation cost is determined to be 9835.762 $, while the carbon emission amounts to 26481.681 kg. The selected solution is highlighted in red in Figure 5 and corresponds to entry number 14 in Table 6. Similar techniques are employed to obtain optimal solutions in other case studies. In case study two, the TOU-DR program is applied, resulting in an operation cost of 9297.363 $ and an emission of 26339.917 kg. On the other hand, case study three involves the implementation of the RTP DR program, which leads to an operation cost of 9610.959 $ and an emission of 25919.747 kg.

The comparative analysis between Case 1 and Case 2 underscores the benefits of the TOU-DR program. In Case 2, the operational costs are curtailed by 5.47%, marking a notable enhancement in the EH system's economic efficiency. Moreover, the model advocates environmental sustainability by registering a 0.53% reduction in emissions, equivalent to 141.764 kg. The outcomes of this case are represented in Table 7. Similarly, a comparison between the results of the first case and the third case demonstrates the benefits of implementing the RTP DR program. In case three, the operation cost experiences a reduction of 2.285%, signifying a noteworthy advancement in the economic aspect of the EH system. Moreover, the proposed model achieves a 2.12% (561.934 kg) decrease in carbon emission, further supporting environmental objectives. The outcomes of this case are represented in Table 8.

4.2. The comparison of the energy flow of the hub in three cases

This section presents a detailed discussion of the optimized EH's outcomes across different scenarios, focusing on power flow, cooling, and heating efficiencies. Case 2 demonstrates the efficacy of the TOU-DRP. The strategic implementation of TOU-DRP not only leads to a decrease in operational costs but also contributes to a reduction in carbon emissions. Figure 6-8 illustrate the energy balance of the power hub in each case, as well as the energy production of each device. The negative values in the diagram are input energy and positive values show output energy for each time period. Figure 6 shows the energy flow in the power hub without DR programs, while Figure 7 shows the energy flow with TOU. By implementing TOU, the gas purchased costs increased from $7382.294 to $7456.332, while the electricity purchased costs decreased from $2388.467 to $1776.031. The GT, when TOU is applied, operates in hour 1 and produces more power in hours 2 and 24 compared to the base case. The DR program and load shifting to off-peak and cheaper hours reduce the number of hours energy needs to be purchased from the main grid from 20 to 10 in case two.

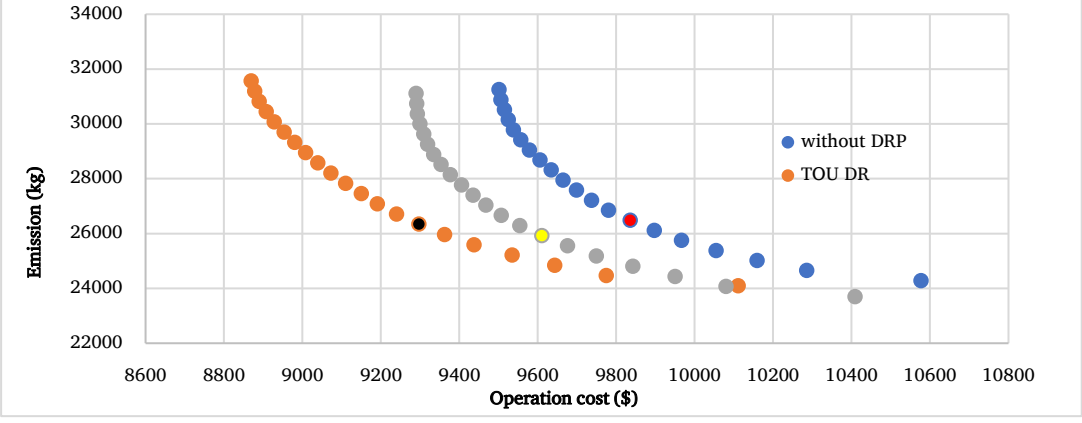

Figure 5. Pareto solutions for scenarios with and without DRP.

Table 6. Pareto results of scenario one (without DRP).

#	Operation cost ($)	Carbon emission (kg	$\psi_1(pu)$	$\psi_2(pu)$	$Min(\psi_1(pu),\psi_2(pu))$
1	9500.732	31247.116	1.00000000	0	0
2	9505.730	30880.544	0.99535629	0.05263159	0.053
3	9514.838	30513.972	0.98689392	0.10526319	0.105
4	9524.622	30147.400	0.97780346	0.15789478	0.158
5	9537.937	29780.828	0.96543231	0.21052638	0.211
6	9556.125	29414.256	0.94853358	0.26315797	0.263
7	9578.279	29047.685	0.92794998	0.31578942	0.316
8	9605.599	28681.113	0.90256658	0.36842101	0.368
9	9633.715	28314.541	0.87644361	0.42105261	0.421
10	9664.468	27947.969	0.84787056	0.47368420	0.474
11	9698.066	27581.397	0.81665419	0.52631580	0.526
12	9736.392	27214.825	0.78104496	0.57894739	0.579
13	9779.835	26848.253	0.74068145	0.63157899	0.632
14	**9835.762**	**26481.681**	**0.68871888**	**0.68421058**	**0.684**
15	9897.165	26115.109	0.63166848	0.73684217	0.632
16	9966.216	25748.537	0.56751222	0.78947377	0.568
17	10054.092	25381.965	0.48586539	0.84210536	0.486
18	10158.776	25015.393	0.38860200	0.89473696	0.389
19	10285.229	24648.821	0.27111273	0.94736855	0.271
20	10577.026	24282.250	0	1	0

Table 7. Pareto results of scenario two (with TOU DRP).

#	Operation cost ($)	Carbon emission (kg	$\psi_1(pu)$	$\psi_2(pu)$	$Min(\psi_1(pu),\psi_2(pu))$
1	8868.649	31569.164	1	0	0
2	8877.768	31195.647	0.99265842	0.04999991	0.050
3	8889.097	30822.129	0.98353761	0.09999996	0.100
4	8907.255	30448.611	0.96891887	0.15000001	0.150
5	8927.953	30075.094	0.95225521	0.19999992	0.200
6	8953.215	29701.576	0.93191713	0.24999997	0.250
7	8979.806	29328.058	0.91050910	0.30000001	0.300
8	9008.038	28954.541	0.88777993	0.34999993	0.350
9	9038.469	28581.023	0.86328037	0.39999997	0.400
10	9072.187	28207.505	0.83613449	0.45000002	0.450
11	9109.833	27833.987	0.80582624	0.50000007	0.500
12	9150.126	27460.470	0.77338693	0.54999998	0.550
13	9190.938	27086.952	0.74052978	0.60000003	0.600
14	9239.505	26713.434	0.70142919	0.65000007	0.650
15	**9297.363**	**26339.917**	**0.65484855**	**0.69999999**	**0.655**
16	9362.414	25966.399	0.60247693	0.75000003	0.602
17	9437.403	25592.881	0.54210436	0.80000008	0.542
18	9533.991	25219.364	0.46434276	0.84999999	0.464
19	9643.077	24845.846	0.37651920	0.90000004	0.377
20	9774.472	24472.328	0.27073498	0.95000009	0.271
21	10110.753	24098.811	0	1	0

Table 8. Pareto results of scenario three (with RTP DRP).

#	Operation cost ($)	Carbon emission (kg	$\psi_1(pu)$	$\psi_2(pu)$	$Min(\psi_1(pu),\psi_2(pu))$
1	9289.634	31107.707	1	0	0
2	9291.128	30737.139	0.99866527	0.04999993	0.050
3	9292.891	30366.570	0.99709022	0.09999999	0.100
4	9299.352	29996.002	0.99131800	0.14999991	0.150
5	9308.657	29625.433	0.98300497	0.19999997	0.200
6	9318.809	29254.864	0.97393523	0.25000003	0.250
7	9334.122	28884.296	0.96025469	0.29999996	0.300
8	9353.085	28513.727	0.94331326	0.35000002	0.350
9	9377.076	28143.159	0.92187984	0.39999995	0.400
10	9405.361	27772.590	0.89661020	0.45000001	0.450
11	9434.747	27402.021	0.87035692	0.50000007	0.500
12	9467.307	27031.453	0.84126801	0.54999999	0.550
13	9506.700	26660.884	0.80607454	0.60000005	0.600
14	9553.922	26290.316	0.76388669	0.64999998	0.650
15	**9610.959**	**25919.747**	**0.71293018**	**0.70000004**	**0.700**
16	9675.206	25549.179	0.65553230	0.74999997	0.656
17	9748.998	25178.610	0.58960697	0.80000003	0.590
18	9841.912	24808.041	0.50659816	0.85000009	0.507
19	9950.031	24437.473	0.41000530	0.90000001	0.410
20	10079.544	24066.904	0.29429916	0.95000007	0.294
21	10408.961	23696.336	0	1	0

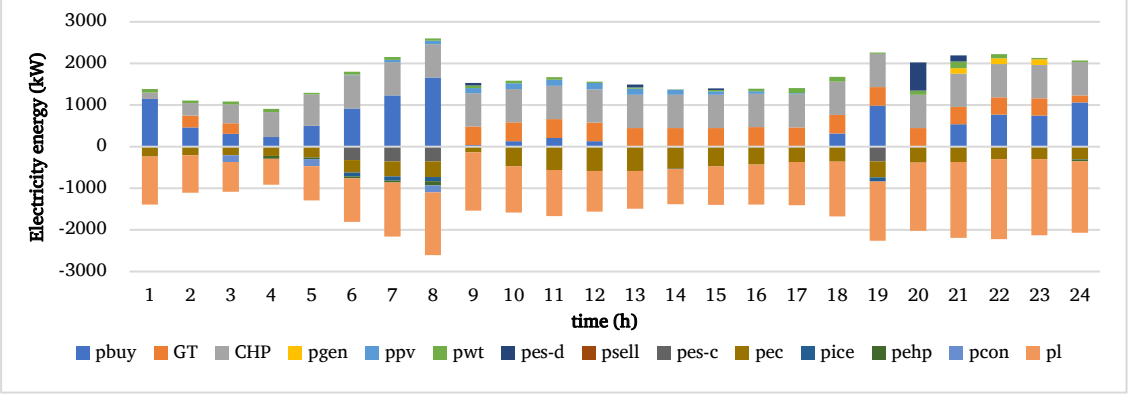

Figure 6. The energy balance of the power hub without DRP.

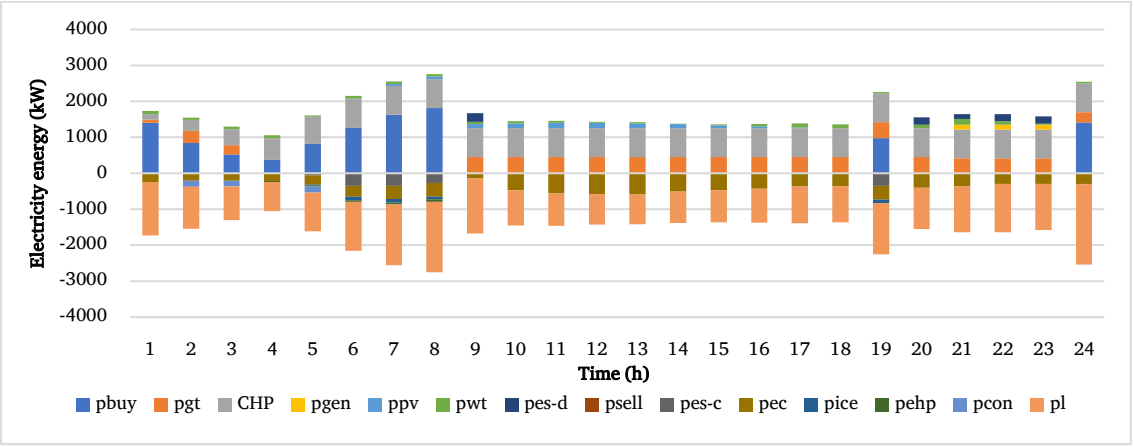

Figure 7. The energy balance of the power hub with TOU-DR.

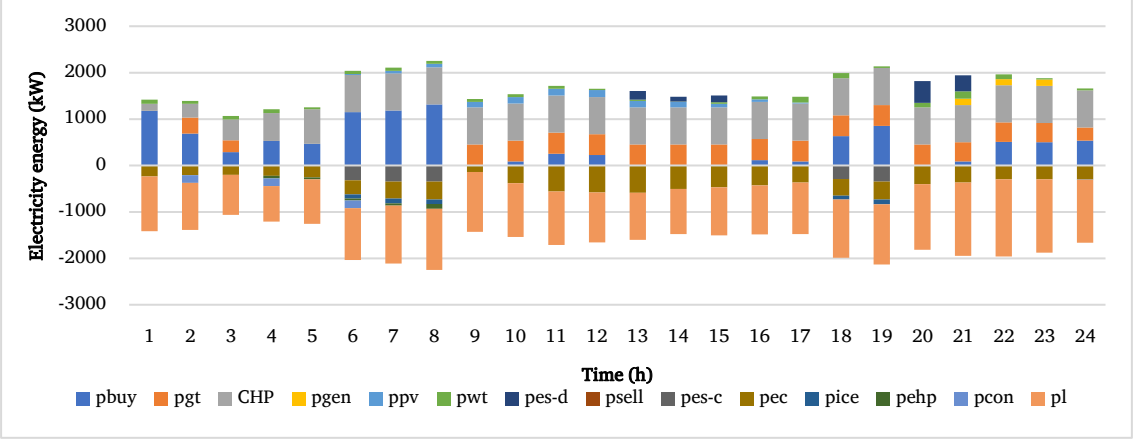

Figure 8. The energy balance of the power hub with RTP DR.

This reduction is due to the multi-objective feature of the model. The power output by the CAES unit remains similar in both cases, but the power consumed by CAES varies based on the imported energy to the EH and the shifted load in hours such as (2:00-8:00). The TOU DRP effectively shifts the load from peak to off-peak and cheaper periods, resulting in lower purchased power costs in case two and a slight decrease in emissions. Additionally, the load is distributed more efficiently. The operational modes of the energy storage (ES) system oscillate between charging and discharging, contingent upon the time of day. For instance, at 16:00, the ES engages in charging mode, whereas it switches to discharging mode during the 13:00-15:00 interval.

In scenarios devoid of a DR Program, the energy discharge rates escalate during peak hours, such as 9:00-21:00, and diminish at 20:00, in response to TOU pricing dynamics. Conversely, in Case 2, with the DRP active, the ES system experiences increased utilization. As a result, the operation time and energy consumed by the EH power are decreased in case two. Figure 8 illustrates the energy flow through the power hub, without and with the RTP DR Program. Upon implementing RTP-DR, the cost of purchased gas rose from $7,382.294 to $7,432.484, while the cost of purchased electricity decreased from $2,388.467 to $2,113.474.

Additionally, the GT generates more power during hours 2, 3, and 24 when RTP DR is applied, as opposed to the base case. In case three time periods in which energy is needed to buy from the main grid are reduced by 1 hour and less power is bought in expensive hours which is caused by the DR program and load shifting to off-peak and cheaper hours. The power output by the CAES unit is similar in both cases which are related to lower gas prices in this time period, but power consumed by CAES is changed based on import energy to the EH and shifted load in hours such as (2:00-4:00-6:00) in RTP DR case. RTP and DRP facilitate the redistribution of loads from peak to more economical off-peak periods. Consequently, in Case 3, the cost of purchased power is marginally reduced, and carbon emissions are decreased by the energy storage system (ES) operating in a charging mode during specific hours, such as 14:00, and switches to a discharging mode during other hours, such as 9:00, in cases where there is no DR program in effect. Additionally, the amount of energy discharged during hours like 13:00, 15:00, 21:00, and 20:00 is increased and decreased, respectively, by RTP-DRP.

The energy flow of the cooling hub is illustrated in Figure 9-11, without and with DRPs, respectively. The primary supplier in the cooling hub is the electric chiller (EC), while the air conditioner (AC) and ice storage chiller (ISC) serve as secondary options during critical hours such as 9:00-20:00 when electricity prices are high. The operation pattern of the absorption chiller remains mostly the same in both case one and case two, except for hour 10, where the cooling output is significantly reduced due to the

implementation of DR. The ISC behaves similarly in both cases, indicating that DRPs have a minimal effect on cooling energy suppliers.

The energy flow of the heating hub is depicted in Figures 12 and 13, without and with TOU DRP, respectively. The main heat suppliers in both cases are the GT, CHP, and EHP. The utilization of heat storage, GT, and CHP remains almost the same in both cases, with only the behavior of EHP differing in each operation hour, particularly at 24:00. The GB produces a minimal amount of adjustment heat, which is similar in both cases one and two.

In the third scenario, the implementation of the RTP DR program yields a reduction in operational costs and a marginal increase in carbon emissions. Figure 8, 11, and 14 depict the power, cooling, and heating energy flows within the EHs, as well as the energy production from each device for Case 3, respectively.

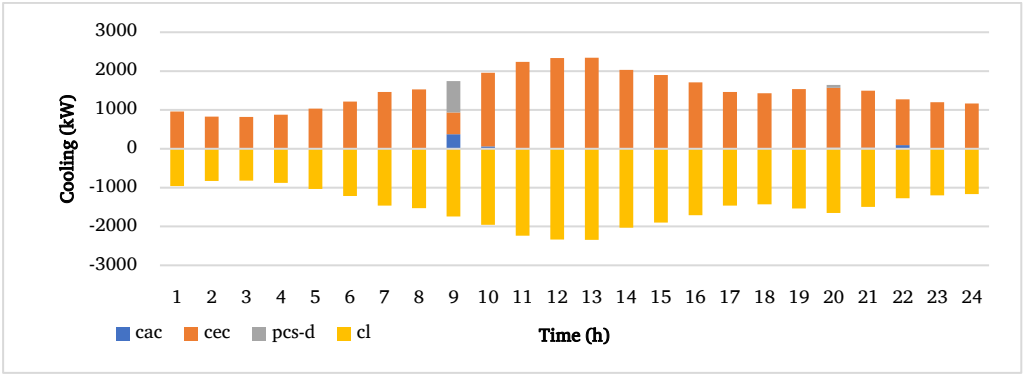

Figure 9. The energy balance of the cooling hub without DRP.

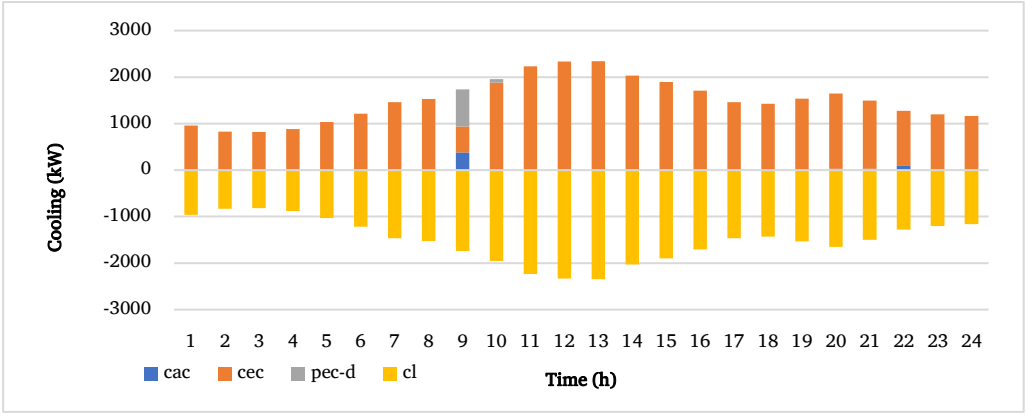

Figure 10. The energy balance of the cooling hub with TOU DR.

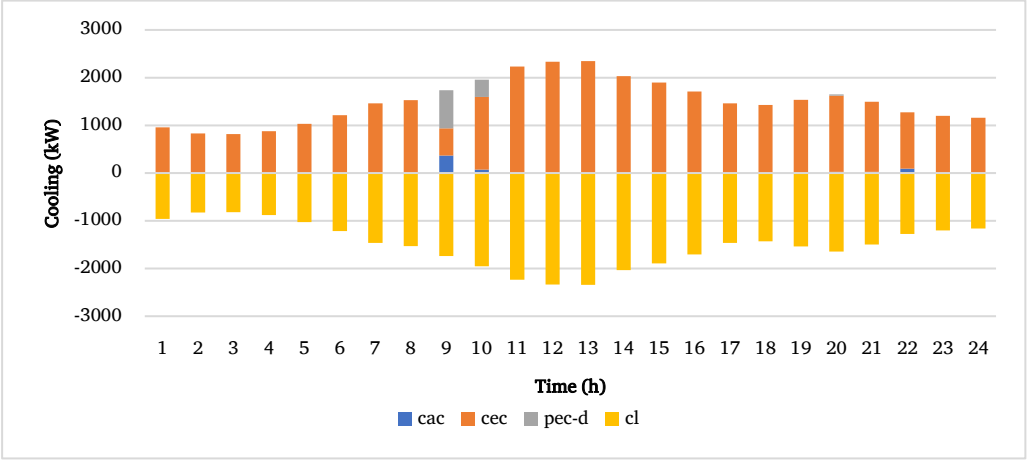

Figure 11. The energy balance of the cooling hub with RTP DR.

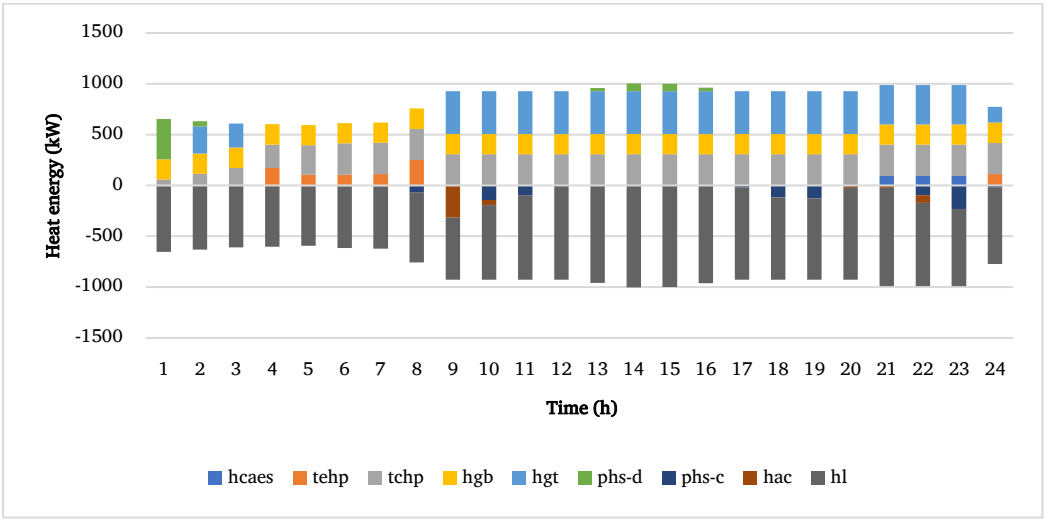

Figure 12. The energy balance of the heat hub without DRP.

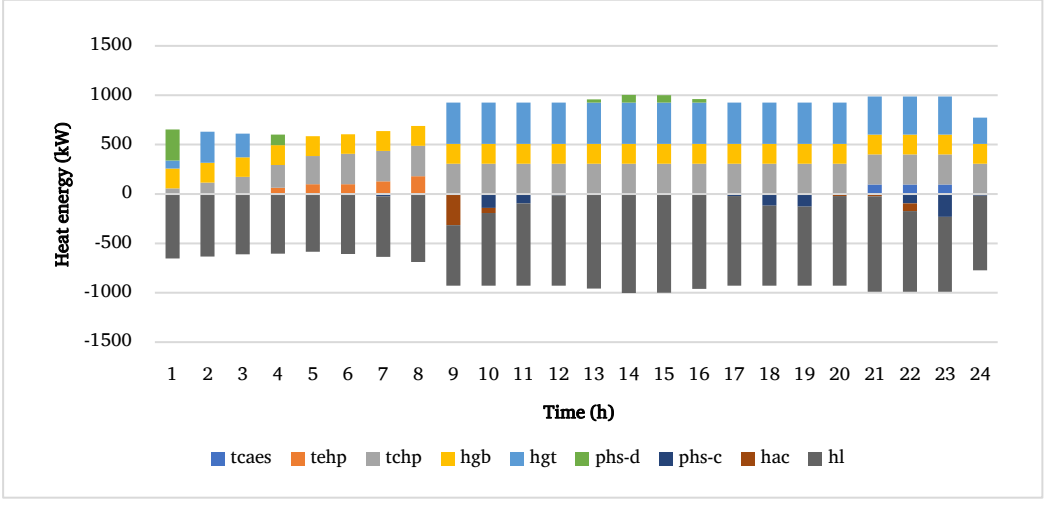

Figure 13. The energy balance of the heat hub with TOU-DR.

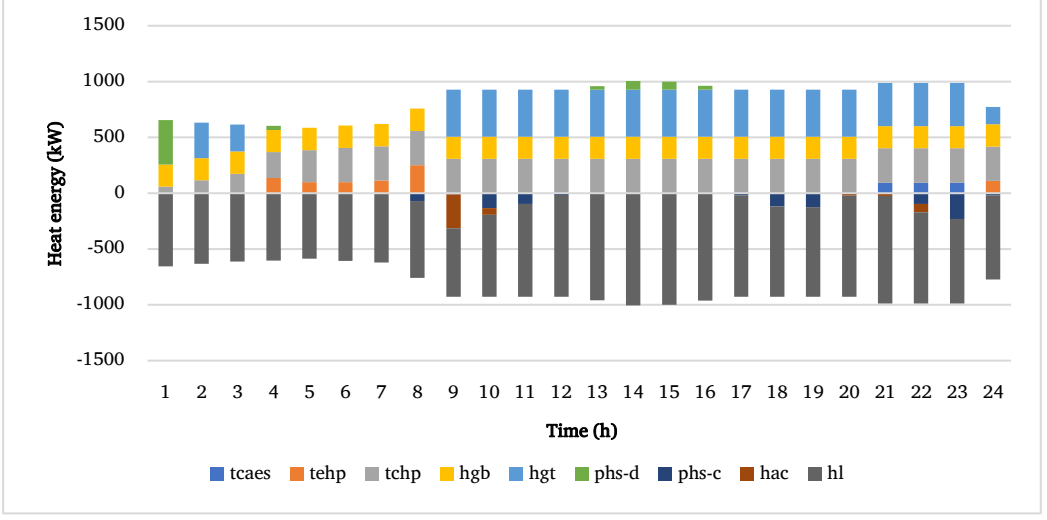

Figure 14. The energy balance of the heat hub with RTP-DR.

Figure 14 represents the energy balance of the cooling hub in the third case. The primary source of cooling is provided by the EC, while AC and ISC serve as alternative options during peak hours, specifically from 9:00 to 10:00, when electricity costs are elevated. The absorption chiller operation pattern is mainly the same in case 1 and case 3 except in hour 10 when the cooling output is increased to 71.290 with applying DR. The ISC works in more hours and produces more cooling in case 3, which proves RTP DR has more effects on cooling energy suppliants compared with RTP DR.

The energy balance of the heating hub for the third case is demonstrated in Figure 14. The use of CHP is almost the same in both cases. The CHP unit's behavior is the same in all three cases, but it is acting very differently in Pareto front solutions with higher priority for operation costs. EHP behavior is different in each of its operation hours especially in (24:00) in DRP. GB produced a minimum amount of its adjustment heat which is similar in all cases. The ES charging and discharge are the same in both cases. The reduction in operation cost and carbon emissions in an EH system can be attributed to two main factors: the decrease in electricity consumption and the increased utilization of storage devices in conjunction with DR programs. Additionally, Figure 15-20 illustrate the charging and discharging of storage devices and the state of ES, CS, and HS in three EHs. It is worth noting that the utilization of storage devices is more prominent in DRP.

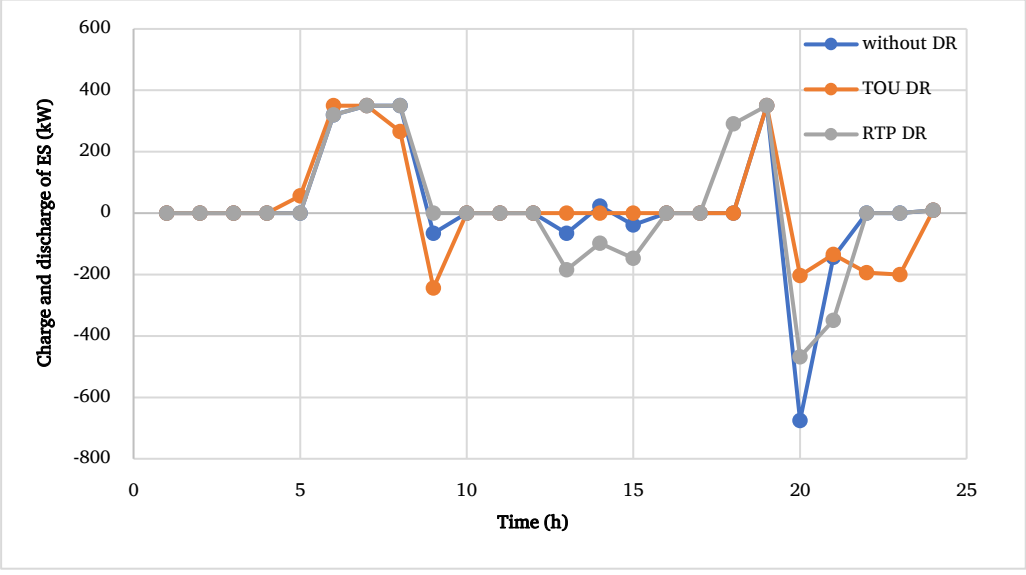

Figure 15. The charging and discharging of electrical storage.

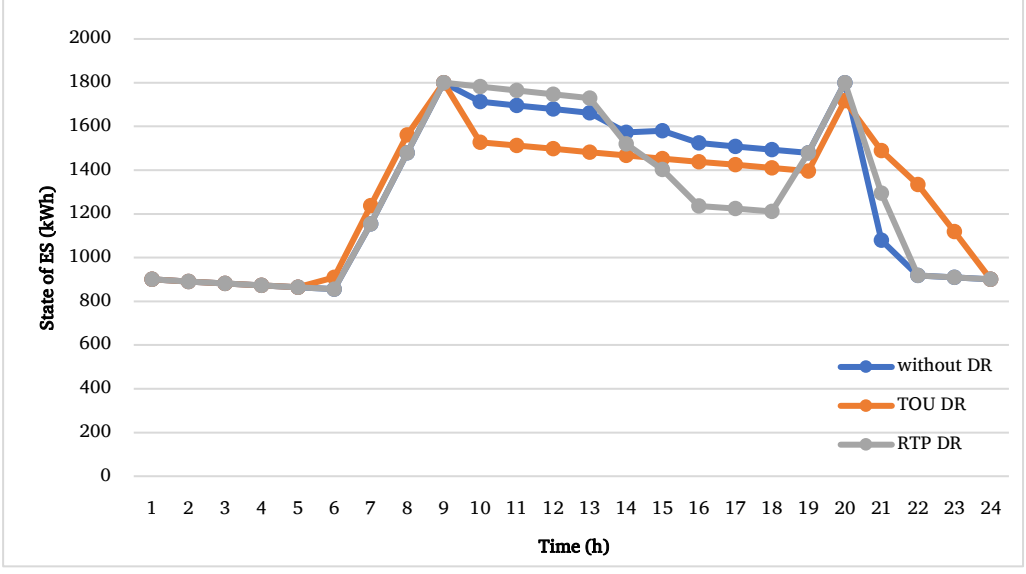

Figure 16. The state of ES.

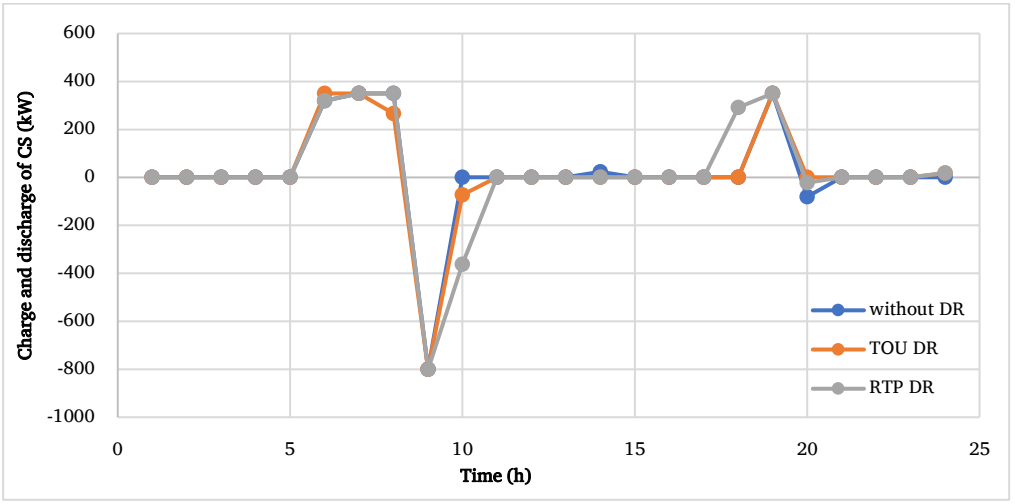

Figure 17. The charging and discharging of cooling storage.

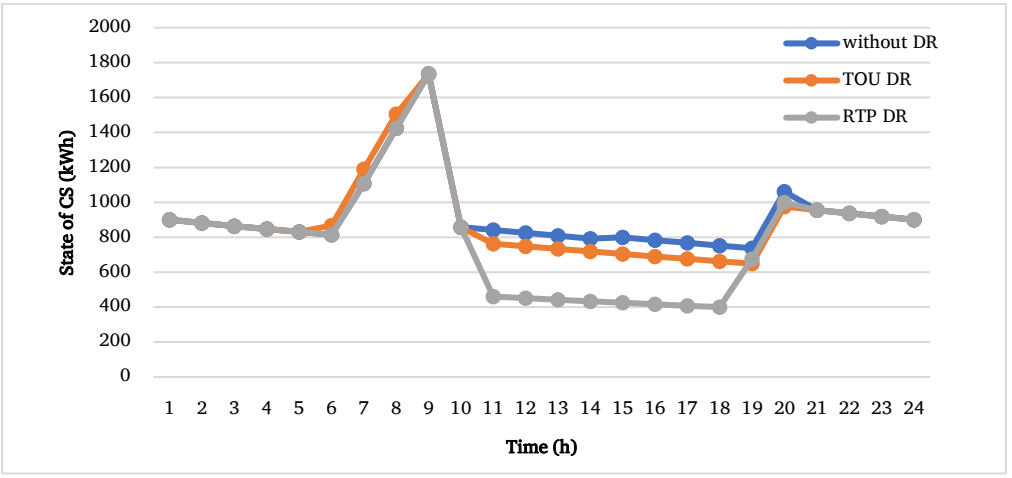

Figure 18. The state of CS.

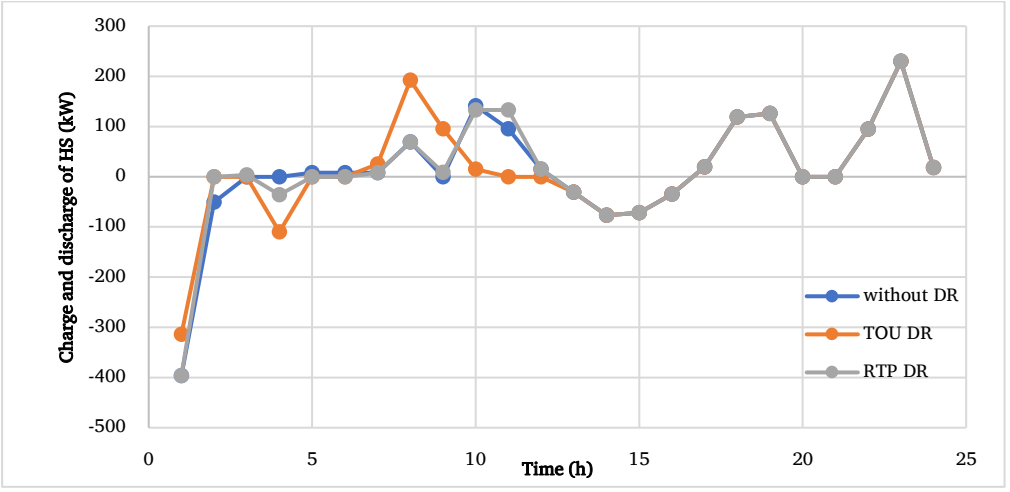

Figure 19. The charging and discharging of heating storage.

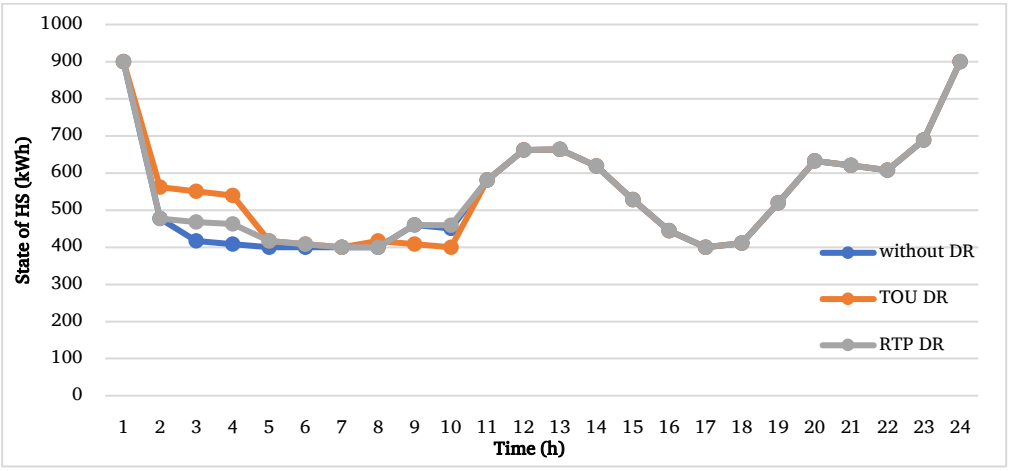

Figure 20. The state of HS.

4.3. The comparison of different CAES storage capacities on objective functions

This section aims to investigate the CAES storage capacity effect on objective functions. For this manner, 6 different levels of capacity are considered for the CAES unit in the model. As shown in Table 9, without considering the CAES unit in the model, operation cost and CO_2 emission are 9879.419 $ and 26407.91 kg, respectively.

Considering the CAES unit in the model with a capacity of 500 kW, operation costs and CO_2 emission are reduced to 9835.76 $ and increased to 26481.7 kg, respectively. As shown in Table 9 and Figure 21 and 22, by increasing CAES unit capacity, operation cost is reduced, and CO_2 emission is increased. For 800 kW and 900kW capacity, operation cost and CO_2 emissions are almost the same, which shows that increasing the capacity of the CAES unit has no benefit for the system. As shown in Figure 21 optimal solution for a minimum amount of emission (number 20 or 21 solution in the Pareto chart) for different CAES capacities are the same. This is due to the CAES unit's CO_2 emission which leads the CAES unit not to operate in these solutions. 500kW CAES capacity is the only capacity that can lead to operation cost and CO_2 emission reduction at the same time compared with 0 capacities for CAES in lower number optimal solutions (number 1 to 13 solutions in Pareto chart) . for example, in a minimum amount of operation cost and emission for 0kW capacity CAES are 9560.456$ and 31367.59kg, and for the 500kW capacity CAES are 9500.732$ and 31247.12kg.

Table 9. Sensitivity analysis of the proposed planning.

CAES capacity (kW)	Objective functions	
	Cost ($)	Pollution (kg)
0	9879.419	26407.91
500	9835.76	26481.7
600	9827.219	26494.1
700	9816.6	26536.52
800	9811.667	26564.52
900	9811.545	26564.86

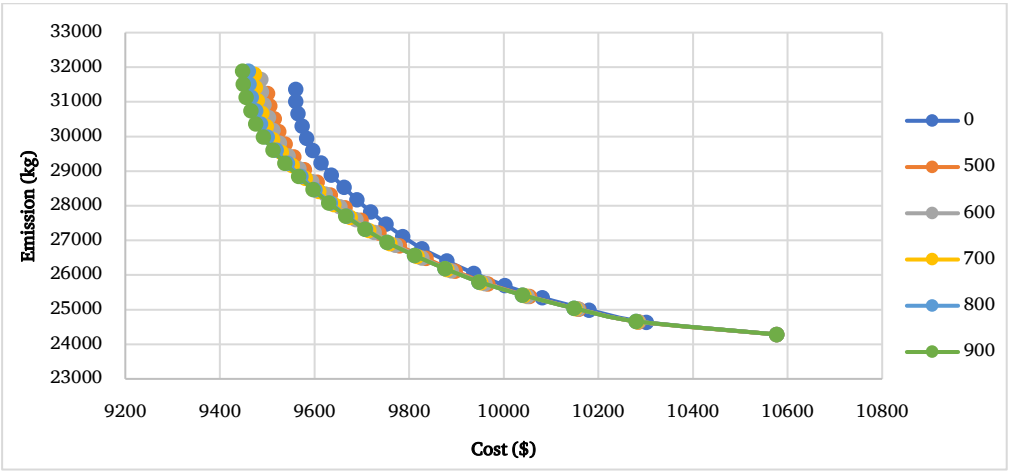

Figure 21. Pareto solutions for different CAES capacity.

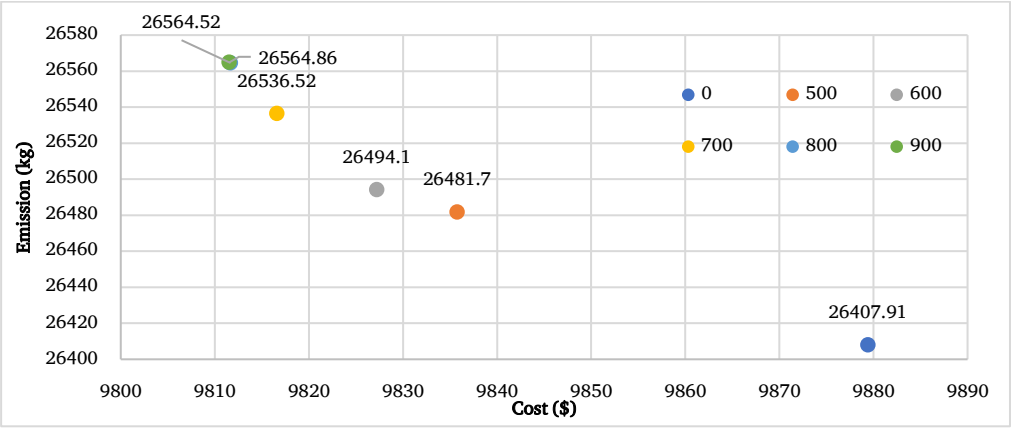

Figure 22. CAES sensitivity analyzed.

5. Conclusion

This paper proposes a comprehensive model of the microenergy grid as an EH system that can provide electricity, heating, and cooling from various sources. The system includes renewable energies, storage devices, and CAES systems. Reduction of operation costs and CO2 emission are investigated in three different cases for the proposed model. Multi-objective model is solved by the augmented epsilon constraint method to obtain Pareto solutions, and the optimal solution is chosen by the max-min fuzzy technique. A good trade-off solution is obtained by the augmented epsilon constraint method in comparison with other methods. TOU and RTP DRs are used to improve the economic and environmental aspects of the proposed EH. Optimal objective functions for the proposed EH are investigated in three cases which are the first case without DRP, the second case with TOU DR, and the third case with RTP DR. In the EH model for case study one without considering any DRP, results for operation cost and carbon emission are 9835.762 $ and 26481.681 kg, respectively. Comparing the results of cases one and two shows that employing TOU-DR causes a 5.47% reduction in operation cost and a 0.53% (141.764kg) decrease in carbon emission. Furthermore, significant improvement has been made by the implementation of TOU-DR for operation costs and a small reduction in CO2 emission. Comparing the results of cases one and three shows that employing RTP DR causes a 2.285% reduction in operation cost and a 2.12% (561.934kg) decrease in carbon emission. Implementation of RTP DR has gained good operation cost and CO2 emission reduction for the proposed model objective functions. Different CAES capacities are applied in the model which shows using a CAES unit mainly will improve operation cost and increase CO2 emission in the proposed model. However, employing a CAES unit with 500kW capacity in some solutions can improve operation cost and CO2 emission, simultaneously.

Nomenclature

t	Time index (h)
C_{ec}^{t}	Output cooling of electrical chiller (kW)
C_{ac}^{t}	Output cooling of absorption chiller (kW)
Pl_{RTP}^{t}	Load demand considering real-time DRP (kW)
Pl_{DR}^{t}	Load demand with considering time of use DRP (kW)
E_{es}^{t}	Stored energy of electricity storage (kWh)
E_{hs}^{t}	Stored energy of heat storage (kWh)
E_{cs}^{t}	The stored energy of the ice storage tank (kWh)
H_{gb}^{t}	Output heat of gas boiler (kW)
H_{gt}^{t}	Waste Heat of gas turbine (kW)

H_{ac}^{t}	Input heat of absorption chiller (kW)
M_{pg}	Gas purchased cost ($)
M_{pe}	Electricity purchased cost ($)
P_{gas}^{t}	Input gas from gas grid (kW) t
P_{ge}^{t}	Input gas of gas turbine (kW)
P_{pv}^{t}	Generated power by PV (kW)
P_{wt}^{t}	Generated power by WT (kW)
P_{gh}^{t}	Input gas of gas boiler (kW)
P_{gt}^{t}	Generated power from gas turbine (kW)
P_{gcaes}^{t}	Input gas of gas CAES (kW)
P_{gchp}^{t}	Input gas of gas CHP (kW)
P_{grid}^{t}	Exchange power between the electricity grid and energy hub system (kW)
P_{buy}^{t}	Import electricity power from the grid (kW)
P_{sell}^{t}	export electricity power to the grid (kW)
P_{grid}^{t}	Input power of chiller (kW)
P_{ice}^{t}	Input power of the ISC's chiller (kW)
$P_{cs,c}^{t}$	Charging cool of ice storage conditioner (kW)
$P_{cs,d}^{t}$	Discharging cool of ice storage conditioner (kW)
$P_{hs,c}^{t}$	Charging heat of heat storage (kW)
$P_{hs,d}^{t}$	Discharging heat of heat storage (kW)
$P_{es,c}^{t}$	Charging power of electricity storage (kW)
$P_{es,d}^{t}$	Discharging power of electricity storage (kW)
SUC	Startup cost of the CHP unit
SDC	shutdown cost of the CHP unit
P_{chp}^{t}, T_{chp}^{t}	Electricity/thermal generation of the CHP
$V_{injected}^{t}$	The energy equivalent of injected air to CAES/combustion chamber
V_{pumped}^{t}	The energy equivalent of pumped air to CAES/combustion chamber

$P^t_{cons.}$, $P^t_{gen.}$	The power consumed/output by/of CAES.
PS^t	The amount of stored energy in the CAES.
T^t_{tr}	Thermal output of the CAES
T^t_{EHP}	Thermal output of the EHP
P^t_{EHP}	Electrical input of the EHP
u^t_{es}	The binary variable of electrical storage is 1 in charging mode otherwise 0
u^t_{hs}	Binary variable of heat storage,1 in charging mode otherwise 0
u^t_{cs}	Binary variable of ISC, 1 in charging mode otherwise 0
COP_{ec}	Coefficient for the performance of electrical chiller
COP_{ice}	Coefficient for the performance of ice storage conditioner (ISC)
COP_{ac}	Coefficient for the performance of absorption chiller
Pl^t	Initial electricity demand (kW)
$E^{\min}_{es}$	Minimum stored energy of electricity storage (kWh)
$E^{\max}_{es}$	Maximum stored energy of electricity storage (kWh)
$E^{\min}_{hs}$	Minimum stored energy of heat storage (kWh)
$E^{\max}_{hs}$	Maximum stored energy of heat storage (kWh)
$E^{\min}_{cs}$	Minimum stored energy of ice storage tank (kWh)
$E^{\max}_{cs}$	Maximum stored energy of ice storage tank (kWh)
E	Elasticity coefficient of RTP demand price
$H^{\max}_{gb}$	Maximum output heat of gas boiler (kW)
$H^{\max}_{ac}$	Maximum input heat of absorption chiller (kW)
$P^{\max}_{es,c}$	Maximum charging power of electricity storage (kW)
$P^{\max}_{hs,c}$	Maximum charging heat of heat storage (kW)
$P^{\max}_{cs,c}$	Maximum charging cool of ISC (kW)
$P^{\max}_{es,d}$	Maximum discharging power of electricity storage (kW)
$P^{\max}_{hs,d}$	Maximum discharging heat of heat storage (kW)
$P^{\max}_{cs,d}$	Maximum discharging cool of ISC (kW)

$P_{gt}^{\max}$	Maximum generated power from gas turbine (kW)
$P_{wt}^{\max}$	Maximum generated power by wind turbine (kW)
$P_{grid}^{\max}$	Maximum exchange power between the electricity grid and energy hub system (kW)
$P_{gas}^{\max}$	Maximum of input gas from gas grid (kW)
$P_{ec}^{\max}$	Maximum input power of chiller (kW)
$P_{ice}^{\max}$	Maximum input power of the ISC's chiller (kW)
$P_{pv}^{\max}$	Maximum generated power by photovoltaic system (kW)
P_g^t	Gas price ($/kWh)
P_{av}	Average electricity demand (kW)
Dn_i , Up_i	Auxiliary variable for modeling MDT and MUT constraints
$\lambda_{RTP}^{\min}$	Minimum amount of RTP ($)
$\lambda_{RTP}^{\max}$	Maximum amount of RTP ($)
λ_{RTP}^t	Real-time pricing ($)
γ^t	Float factor of RTP
W_d	Integrated of all energy demand (kW)
β_e	Equivalent emission coefficient of electricity (kg/kWh)
β_g	Equivalent emission coefficient of natural gas (kg/kWh)
$\eta_{es,c}$	Charging efficiency of electrical storage
$\eta_{hs,c}$	Charging efficiency of heating storage
$\eta_{cs,c}$	Charging efficiency of cooling storage
$\eta_{es,d}$	Discharging efficiency of electrical storage
$\eta_{hs,d}$	Discharging efficiency of heating storage
$\eta_{cs,d}$	Discharging efficiency of cooling storage
η_{ge}	Gas turbine efficiency for generating power
$\eta_{gh,gb}$	Gas boiler efficiency for generating heat
$\eta_{gh,gt}$	Gas turbine efficiency for generating heat
η_t	Transformer efficiency

η_{he}	Efficiency of heat exchanger
δ_{es}	Energy loss ratio of electrical storage
δ_{hs}	Energy loss ratio of heat storage
δ_{cs}	Energy loss ratio of ISC
$P_{chp}^{\max}$, $P_{chp}^{\min}$	Upper/lower limits of the CHP units outputs.
HV	Heat value of the natural gas
SU, SD	The start-up and shut-down cost of CHP
η_{He}	Efficiency of the CHP heat exchanger
HPR	Heat to power ratio of the CHP unit.
$P^{Ramp-up}$	Ramp-up rate of the CHP
$P^{Ramp-down}$	Ramp-down rate of the CHP
η_{chp}	Electrical efficiency of the CHP unit.
e^{i}, e^{p}	The efficiency of injected/produced power of the CAES system.
$V_{pumped}^{\max}$	Maximum level of pumped air from storage to combustion chamber
$V_{pumped}^{\min}$	Minimum level of pumped air from storage to combustion chamber
$V_{ingected}^{\max}$	Maximum level of injected air into the CAES system
$V_{ingected}^{\min}$	Minimum level of injected air into the CAES system
$PS^{\min}$	Minimum level CAES
$PS^{\max}$	Maximum level CAES
COP_{EHP}	Coefficient of performance of the EHP.

References

[1] T. Ding, W. Jia, et al., "Review of Optimization Methods for Energy Hub Planning, Operation, Trading, and Control," *IEEE Transactions on Sustainable Energy*, vol. 13, no. 3, pp. 1802–1818, 2022.

[2] P. Hajiamoosha, A. Rastgou, S. Bahramara, and S. M. Bagher Sadati, "Stochastic Energy Management in a Renewable Energy-Based Microgrid Considering Demand Response Program," *International Journal of Electrical Power & Energy Systems*, vol. 129, 106791, 2021.

[3] A. Rastgou, "Distribution Network Expansion Planning: An Updated Review of Current Methods and New Challenges," *Renewable and Sustainable Energy Reviews*, vol. 189, 114062, 2024.

[4] K. Gholami, S. Karimi, and A. Rastgou, "Fuzzy Risk-Based Framework for Scheduling of Energy Storage Systems in Photovoltaic-Rich Networks," *Journal of Energy Storage*, vol. 52, 104902, 2022.

[5] A. A. Eladl, M. I. El-Afifi, M. M. El-Saadawi, and B. E. Sedhom, "A Review on Energy Hubs: Models, Methods, Classification, Applications, and Future Trends," *Alexandria Engineering Journal*, vol. 68, pp. 315–342, 2023.

[6] T. Ha, Y. Xue, et al., "Optimal Operation of Energy Hub Based Micro-Energy Network with Integration of Renewables and Energy Storages," *Journal of Modern Power Systems and Clean Energy*, vol. 10, no. 1, pp. 100–108, 2022.

[7] X. Zhou, Z. Ma, S. Zou, J. Zhang, and Y. Guo, "Distributed Energy Management of Double-Side Multienergy Systems Via Sub-Gradient Averaging Consensus," *IEEE Transactions on Smart Grid*, vol. 14, no. 2, pp. 979–995, 2023.

[8] A. Rastgou, J. Moshtagh, and S. Bahramara, "Probabilistic Power Distribution Planning Using Multi-Objective Harmony Search Algorithm," *Journal of Operation and Automation in Power Engineering*, vol. 6, no. 1, pp. 111-125, 2018.

[9] M. Jadidbonab, E. Babaei, and B. Mohammadi-ivatloo, "CVaR-Constrained Scheduling Strategy for Smart Multi Carrier Energy Hub Considering Demand Response and Compressed Air Energy Storage," *Energy*, vol. 174, pp. 1238–1250, 2019.

[10] M. Rastegar, M. Fotuhi-Firuzabad, and M. Lehtonen, "Home Load Management in a Residential Energy Hub," *Electric Power Systems Research*, vol. 119, pp. 322–328, 2015.

[11] A. Hussain, S. M. Arif, M. Aslam, and S. D. A. Shah, "Optimal Siting and Sizing of Tri-Generation Equipment for Developing an Autonomous Community Microgrid Considering Uncertainties," *Sustainable Cities and Society*, vol. 32, pp. 318–330, 2017.

[12] F. Jabari, S. Nojavan, and B. Mohammadi Ivatloo, "Designing and Optimizing a Novel Advanced Adiabatic Compressed Air Energy Storage and Air Source Heat Pump Based M-Combined Cooling, Heating and Power System," *Energy*, vol. 116, pp. 64–77, 2016.

[13] X. Chen, G. Gong, Z. Wan, C. Zhang, and Z. Tu, "Performance Study of a Dual Power Source Residential CCHP System Based on PEMFC and PTSC," *Energy Conversion and Management*, vol. 119, pp. 163–176, 2016.

[14] M. Geidl, G. Koeppel, et al., "Energy Hubs for the Future," *IEEE Power and Energy Magazine*, vol. 5, no. 1, pp. 24–30, 2007.

[15] M. Geidl, and G. Andersson, "Optimal Coupling of Energy Infrastructures," *2007 IEEE Lausanne Power Tech*, 2007.

[16] S. Bahrami, and F. Safe, "A Financial Approach to Evaluate an Optimized Combined Cooling, Heat and Power System," *Energy and Power Engineering*, vol. 05, no. 05, pp. 352–362, 2013.

[17] D. Xu, Q. Wu, et al., "Distributed Multi-Energy Operation of Coupled Electricity, Heating, and Natural Gas Networks," *IEEE Transactions on Sustainable Energy*, vol. 11, no. 4, pp. 2457–2469, 2020.

[18] M. Rastegar, and M. Fotuhi-Firuzabad, "Load Management in a Residential Energy Hub with Renewable Distributed Energy Resources," *Energy and Buildings*, vol. 107, pp. 234–242, 2015.

[19] M. C. Bozchalui, S. A. Hashmi, H. Hassen, C. A. Canizares, and K. Bhattacharya, "Optimal Operation of Residential Energy Hubs in Smart Grids," *IEEE Transactions on Smart Grid*, vol. 3, no. 4, pp. 1755–1766, 2012.

[20] M. Moeini-Aghtaie, A. Abbaspour, M. Fotuhi-Firuzabad, and P. Dehghanian, "Optimized Probabilistic PHEVs Demand Management in the Context of Energy Hubs," *IEEE Transactions on Power Delivery*, vol. 30, no. 2, pp. 996–1006, 2015.

[21] S. Zheng, Y. Sun, et al., "Incentive-Based Integrated Demand Response for Multiple Energy Carriers Considering Behavioral Coupling Effect of Consumers," *IEEE Transactions on Smart Grid*, vol. 11, no. 4, pp. 3231–3245, 2020.

[22] M. Majidi, and K. Zare, "Integration of Smart Energy Hubs in Distribution Networks Under Uncertainties and Demand Response Concept," *IEEE Transactions on Power Systems*, vol. 34, no. 1, pp. 566–574, 2019.

[23] M. Mazidi, A. Zakariazadeh, S. Jadid, and P. Siano, "Integrated Scheduling of Renewable Generation and Demand Response Programs in a Microgrid," *Energy Conversion and Management*, vol. 86, pp. 1118–1127, 2014.

[24] S. Nojavan, and H. A. Aalami, "Stochastic Energy Procurement of Large Electricity Consumer Considering Photovoltaic, Wind-Turbine, Micro-Turbines, Energy Storage System in the Presence of Demand Response Program," *Energy Conversion and Management*, vol. 103, pp. 1008–1018, 2015.

[25] P. Mancarella, and G. Chicco, "Real-Time Demand Response from Energy Shifting in Distributed Multi-Generation," *IEEE Transactions on Smart Grid*, vol. 4, no. 4, pp. 1928–1938, 2013.

[26] B. Yan, S. Xue, Y. Li, J. Duan, and M. Zeng, "Gas-Fired Combined Cooling, Heating and Power (CCHP) in Beijing: A Techno-Economic Analysis," *Renewable and Sustainable Energy Reviews*, vol. 63, pp. 118–131, 2016.

[27] K. Saberi, H. Pashaei-Didani, R. Nourollahi, K. Zare, and S. Nojavan, "Optimal Performance of CCHP Based Microgrid Considering Environmental Issue in the Presence of Real Time Demand Response," *Sustainable Cities and Society*, vol. 45, pp. 596–606, 2019.

[28] D. K. Critz, S. Busche, and S. Connors, "Power Systems Balancing with High Penetration Renewables: The Potential of Demand Response in Hawaii," *Energy Conversion and Management*, vol. 76, pp. 609–619, 2013.

[29] L. Guo, W. Liu, J. Cai, B. Hong, and C. Wang, "A Two-Stage Optimal Planning and Design Method for Combined Cooling, Heat and Power Microgrid System," *Energy Conversion and Management*, vol. 74, pp. 433–445, 2013.

[30] Z. Tan, L. Ju, et al., "The Optimization Model for Multi-Type Customers Assisting Wind Power Consumptive Considering Uncertainty and Demand Response Based on Robust Stochastic Theory," *Energy Conversion and Management*, vol. 105, pp. 1070–1081, 2015.

[31] H. Aalami, M. P. Moghaddam, and G. Yousefi, "Demand Response Modeling Considering Interruptible/Curtailable Loads and Capacity Market Programs," *Applied Energy*, vol. 87, no. 1, pp. 243–250, 2010.

[32] E. Drury, P. Denholm, and R. Sioshansi, "The Value of Compressed Air Energy Storage in Energy and Reserve Markets," *Energy*, vol. 36, no. 8, pp. 4959–4973, 2011.

[33] R. Rezaeipour, and A. Zahedi, "Multi-Objective Based Economic Operation and Environmental Performance of PV-Based Large Industrial Consumer," *Solar Energy*, vol. 157, pp. 227–235, 2017.

[34] S. Nojavan, M. Majidi, and N. N. Esfetanaj, "An Efficient Cost-Reliability Optimization Model for Optimal Siting and Sizing of Energy Storage System in a Microgrid in the Presence of Responsible Load Management," *Energy*, vol. 139, pp. 89–97, 2017.

[35] S. Nojavan, M. Majidi, A. Najafi-Ghalelou, M. Ghahramani, and K. Zare, "A Cost-Emission Model for Fuel Cell/PV/Battery Hybrid Energy System in the Presence of Demand Response Program: E-Constraint Method and Fuzzy Satisfying Approach," *Energy Conversion and Management*, vol. 138, pp. 383–392, 2017.

Declaration of competing interest

The authors declare that they have no known competing financial interests or personal relationships that could have appeared to influence the work reported in this paper. The ethical issues, including plagiarism, informed consent, misconduct, data fabrication and/or falsification, double publication and/or submission, redundancy, have been completely observed by the authors.

Bibliography

Pouria Hajiamoosha is a dedicated researcher in the field of electrical power engineering, with a focus on optimization and the management of microgrids and energy systems. He holds a Master's degree in Electrical Power Engineering from the Islamic Azad University, Science and Research Branch of Kermanshah, as well as a Bachelor's degree in Electrical and Electronics Engineering from the Islamic Azad University.
Email: poorya.php@gmail.com
ORCID: 0009-0009-3345-8986
Contribution Statement: Formal analysis, Methodology, Software, Roles/Writing - original draft, Writing-review & editing.

Abdollah Rastgou holds a Bachelor's, Master's, and Ph.D. degree in Power Electrical Engineering. He completed his Bachelor's degree at Tabriz University and went on to earn both his Master's and Ph.D. degrees with honors from Kurdistan University in Sanandaj. Dr. Rastgou has a keen interest in power system planning, bi-level planning, and renewable resource planning. His academic journey reflects a strong commitment to advancing the field of electrical engineering, particularly in optimizing power systems for sustainability and efficiency.
Email: abdollah.rastgou@iau.ac.ir
ORCID: 0000-0002-8620-2185
Contribution Statement: Conceptualization, Data curation, Formal analysis, Funding acquisition, Investigation, Methodology, Project administration, Resources, Software, Supervision, Validation, Visualization,

Hadi Afshar received the B.Sc. and the M.Sc. degrees in electrical engineering from the Semnan University, Semnan, Iran, in 2010 and 2013, respectively. His research interests include smart grids, renewable energy systems, energy management, power system operation, optimization, and planning.
Email: Haaf963@gmail.com
ORCID: 0009-0000-2799-367X
Contribution Statement: Formal analysis, Software, Writing-review & editing.